The Astrophysical Journal, 707:1729–1739, 2009 December 20 doi:10.1088/0004-637X/707/2/1729

BLAST: RESOLVING THE COSMIC SUBMILLIMETER BACKGROUND

Gaelen Marsden[1], Peter A. R. Ade[2], James J. Bock[3], Edward L. Chapin[1], Mark J. Devlin[4], Simon R. Dicker[4], Matthew Griffin[2], Joshua O. Gundersen[5], Mark Halpern[1], Peter C. Hargrave[2], David H. Hughes[6], Jeff Klein[4], Philip Mauskopf[2], Benjamin Magnelli[7], Lorenzo Moncelsi[2], Calvin B. Netterfield[8,9], Henry Ngo[1], Luca Olmi[10,11], Enzo Pascale[2], Guillaume Patanchon[12], Marie Rex[4], Douglas Scott[1], Christopher Semisch[4], Nicholas Thomas[5], Matthew D. P. Truch[4], Carole Tucker[2], Gregory S. Tucker[13], Marco P. Viero[8], and Donald V. Wiebe[1,9]
[1] Department of Physics & Astronomy, University of British Columbia, 6224 Agricultural Road, Vancouver, BC V6T 1Z1, Canada; gmarsden@phas.ubc.ca
[2] School of Physics & Astronomy, Cardiff University, 5 The Parade, Cardiff, CF24 3AA, UK
[3] Jet Propulsion Laboratory, Pasadena, CA 91109-8099, USA
[4] Department of Physics & Astronomy, University of Pennsylvania, 209 South 33rd Street, Philadelphia, PA 19104, USA
[5] Department of Physics, University of Miami, 1320 Campo Sano Drive, Coral Gables, FL 33146, USA
[6] Instituto Nacional de Astrofísica Óptica y Electrónica (INAOE), Aptdo. Postal 51 y 72000 Puebla, Mexico
[7] Laboratoire AIM, CEA/DSM-CNRS-Université Paris Diderot, IRFU/Service d'Astrophysique, Bât. 709, CEA-Saclay, F-91191 gif-sur-Yvette Cédex, France
[8] Department of Astronomy & Astrophysics, University of Toronto, 50 St. George Street, Toronto, ON M5S 3H4, Canada
[9] Department of Physics, University of Toronto, 60 St. George Street, Toronto, ON M5S 1A7, Canada
[10] Physics Department, University of Puerto Rico, Rio Piedras Campus, Box 23343, UPR station, Puerto Rico 00931, USA
[11] INAF, Osservatorio Astrofisico di Arcetri, Largo E. Fermi 5, I-50125, Firenze, Italy
[12] Université Paris Diderot, Laboratoire APC, 10, rue Alice Domon et Léonie Duquet 75205 Paris, France
[13] Department of Physics, Brown University, 182 Hope Street, Providence, RI 02912, USA
Received 2009 April 8; accepted 2009 August 6; published 2009 December 7

ABSTRACT

The Balloon-borne Large Aperture Submillimeter Telescope (BLAST) has made 1 deg^2, deep, confusion-limited maps at three different bands, centered on the Great Observatories Origins Deep Survey South Field. By calculating the covariance of these maps with catalogs of 24 μm sources from the Far-Infrared Deep Extragalactic Legacy Survey, we have determined that the total submillimeter intensities are 8.60 ± 0.59, 4.93 ± 0.34, and 2.27 ± 0.20 nW m^{-2} sr^{-1} at 250, 350, and 500 μm, respectively. These numbers are more precise than previous estimates of the cosmic infrared background (CIB) and are consistent with 24 μm-selected galaxies generating the full intensity of the CIB. We find that the fraction of the CIB that originates from sources at $z \geqslant 1.2$ increases with wavelength, with 60% from high-redshift sources at 500 μm. At all BLAST wavelengths, the relative intensity of high-z sources is higher for 24 μm-faint sources than that for 24 μm-bright sources. Galaxies identified as active galactic nuclei (AGNs) by their Infrared Array Camera colors are 1.6–2.6 times brighter than the average population at 250–500 μm, consistent with what is found for X-ray-selected AGNs. BzK-selected galaxies are found to be moderately brighter than typical 24 μm-selected galaxies in the BLAST bands. These data provide high-precision constraints for models of the evolution of the number density and intensity of star-forming galaxies at high redshift.

Key words: cosmology: observations – diffuse radiation – galaxies: evolution – galaxies: starburst – submillimeter

Online-only material: color figure

1. INTRODUCTION

A decade ago, a uniform cosmic infrared background (CIB) radiation was discovered in Far-Infrared Absolute Spectrophotometer (FIRAS) data from the *Cosmic Background Explorer* (*COBE*) by Puget et al. (1996), and later confirmed by Fixsen et al. (1998). The background, which peaks in intensity at a wavelength of ≈ 200 μm, is as bright as all the optical light in the universe (Hauser & Dwek 2001). It is presumed to be thermal reradiation of optical and ultraviolet (UV) starlight absorbed by dust grains. At around the same time as the discovery of the CIB, observations with the Submillimetre Common-User Bolometer Array (SCUBA; Holland et al. 1999) at the James Clerk Maxwell Telescope revealed a population of dusty high-redshift starburst galaxies forming stars at a rate of $\sim$1000 $M_\odot$ yr^{-1} (Blain et al. 1998; Hughes et al. 1998; Barger et al. 1998).

Over the ensuing decade, a substantial effort has been devoted to understanding the implications of this background radiation, and the task has not been easy. Only the few brightest submillimeter galaxies are visible with SCUBA in blank fields above the confusion limit, and these comprise a small fraction of the total CIB at 850 μm (e.g., Hughes et al. 1998; Scott et al. 2002; Borys et al. 2003; Coppin et al. 2006). Full understanding relies on statistical measures of submillimeter galaxies too weak to be detected individually. Attempts to probe the contribution to the CIB by faint sources have been made by looking at objects lensed by clusters (Cowie et al. 2002; Smail et al. 2002; Knudsen et al. 2008). Knudsen et al. (2008) have resolved 100% of the 850 μm background by reaching unlensed flux density limits of 0.1 mJy, but the reliability of the lensing inversion introduces uncertainty in the estimate, and direct detection of these sources is desirable. Furthermore, the CIB signal peaks at wavelengths where the atmosphere is opaque and has dropped by almost 2 orders of magnitude before it reaches the reliable atmospheric window SCUBA exploits. The bulk of the CIB is not visible from the ground.

Since both the numerical density and the emission spectra of galaxies evolve with cosmic epoch, the CIB is a convolution of these evolution functions for a wide range of galaxy types. Because of this, the shape of the CIB contains a wealth of information about the history of star formation. However, working from measurements at only one wavelength, the convolution cannot be inverted to extract an evolution function.

One expects a different mixture of galaxy types, and a different redshift distribution, to emerge from observations of the CIB at different wavelengths. Measurements at several wavelengths are therefore required to constrain models of these underlying distributions.

The Balloon-borne Large Aperture Submillimeter Telescope (BLAST) was designed to carry out the program of characterizing the CIB over a range of wavelengths near its peak. We report here on the success of that program. BLAST has produced deep, confusion-limited maps at three wavelengths (250, 350, and 500 μm), where the CIB produces substantial flux density, and we have used a uniform and carefully constructed catalog of 24 μm-selected galaxies (Magnelli et al. 2009) whose intensities we can find statistically in the BLAST data. These data bridge the gap between similar analyses at shorter wavelengths, using data from the *Spitzer Space Telescope* (e.g., Dole et al. 2006), and at longer wavelengths, using data from SCUBA (e.g., Wang et al. 2006; Serjeant et al. 2008).

Devlin et al. (2009) established that the full intensity of the CIB is statistically resolved into flux density produced by identifiable 24 μm-selected galaxies. In this paper, we examine the relation in more detail by dividing the 24 μm catalogs by brightness and color. A companion paper by Pascale et al. (2009) uses spectroscopic and photometric redshifts to constrain the star formation rate history. E. L. Chapin et al. (2009, in preparation) will explore the implications of these new BLAST results on our understanding of models of galaxy evolution.

We analyze these high signal-to-noise ratio (S/N) BLAST maps of confusion using techniques that differ from those appropriate for catalogs of isolated point sources; we use the covariances between our maps and external catalogs, a technique known as "stacking," to measure the background. Similarly, Devlin et al. (2009) and Patanchon et al. (2009) use a "$P(D)$" fluctuation analysis, rather than counts of individual sources, to provide the most accurate measurements of the underlying source counts, while Viero et al. (2009) study correlations in the background. The possibility of determining number counts, spectral energy distributions, and clustering biases directly from correlations in the maps without the requirement to first extract a catalog of point sources was pointed out by Knox et al. (2001).

The layout of this paper is as follows. In Section 2, the BLAST observations and external data are described. In Section 3, we develop the stacking formulae for measuring the contribution to the total surface brightness detected in a map produced at positions from an external catalog. Finally, in Section 4 we use 24 μm and optical catalogs, and subsets based on color cuts to determine the total CIB measured by BLAST, as well as the relative contributions of low- and high-redshift sources, active galactic nuclei (AGNs), and BzK galaxies. Additionally, we include an analysis of deep extragalactic SCUBA 850 μm observations, similar to those used by Wang et al. (2006).

2. OBSERVATIONS

2.1. BLAST

BLAST is a 1.8 m stratospheric balloon-borne telescope that operates at an altitude of approximately 35 km, above most of the opaque atmospheric water vapor that renders observations at all but a few narrow submillimeter bands from the ground impossible. Observations are simultaneously undertaken with three broadband bolometric imaging arrays with central wavelengths 250, 350, and 500 μm; this camera is a prototype of the Spectral and Photometric Imaging Receiver (SPIRE) for *Herschel* (Griffin et al. 2007).

We use data from the 11-day BLAST flight in 2006 from McMurdo Station, Antarctica. The under-illuminated BLAST primary produced nearly diffraction-limited beams with full width at half-maxima (FWHMs) of 36″, 42″, and 60″ in each band, respectively. This successful flight produced significantly deeper and wider area extragalactic maps than existing 350 and 450 μm ground-based observations, and the first 250 μm maps, near the peak in the CIB. Deep and wide blank-field surveys were conducted in the Great Observatories Origins Deep Survey South (GOODS-S) field, which we label BLAST GOODS-S Deep (BGS-Deep) and BLAST GOODS-S Wide (BGS-Wide), respectively. These maps are centered on the Chandra Deep Field South. A coverage map is shown in Pascale et al. (2009). A second intermediate-depth field near the South Ecliptic Pole, which will be the subject of a separate study, was also observed. In addition, several low-redshift clusters and high-redshift radio galaxies were targeted to sample biased star-forming regions of the universe. Further details on the instrument may be found in Pascale et al. (2008), and the flight performance and calibration for the 2006 flight are provided in Truch et al. (2009).

In this paper, we focus on the deepest BLAST maps of BGS-Deep[14] which cover an area of approximately 0.8 deg^2 (Devlin et al. 2009) and completely encompass the Extended Chandra Deep Field South (ECDF-S), which in turn encompasses the smaller GOODS-S and Hubble Ultra Deep Field South fields. The maps in all BLAST bands are confusion limited, such that instrumental noise itself contributes only a fraction (∼50%, see below) to the rms of the map, and therefore provide high-S/N measurements of the spatial variations in the intensity of the CIB.

All BLAST time-stream detector data are reduced using a common pipeline to identify spikes, correct time-varying detector responsivities, and deconvolve the lag induced by thermal time constants for the bolometers. Maps are produced from a combination of these cleaned data with the pointing solution using a maximum-likelihood algorithm (Patanchon et al. 2008). The absolute calibration is based on regular observations of the evolved star VY CMa, which results in uncertainties of approximately 10% that are strongly correlated between bands (Truch et al. 2009). The resulting maps may be thought of as the optimal weighting of the data on all spatial scales such that both point sources and diffuse structures are accurately reproduced within the limitations of the data. However, while all spatial frequencies (inverse spatial scales) from the mean level up to the Nyquist frequency are estimated, the largest scales (including the absolute brightness) are not well constrained due to detector drift and other systematics. We have therefore suppressed all scales larger than approximately 9′, 7.′5, and 8′ at 250, 350, and 500 μm, respectively—this procedure explicitly sets the mean of each map to zero.[15]

We show in Figure 1 the noise properties of the 500 μm BGS-Deep map. We plot the distribution of the ratio of map pixel values to instrumental noise, $\sigma_{\rm inst}$, estimated by the map maker, which propagates uncertainties in the time-domain detector noise power spectra. The distribution is well described by a Gaussian with an excess at positive flux density, due to bright sources in the map. The shape of the histogram is due to

[14] The BLAST maps used in this paper are available for downloading at http://blastexperiment.info/.

[15] The filter is, in practice, anisotropic, with greater suppression of the more poorly constrained modes orthogonal to the scan direction.

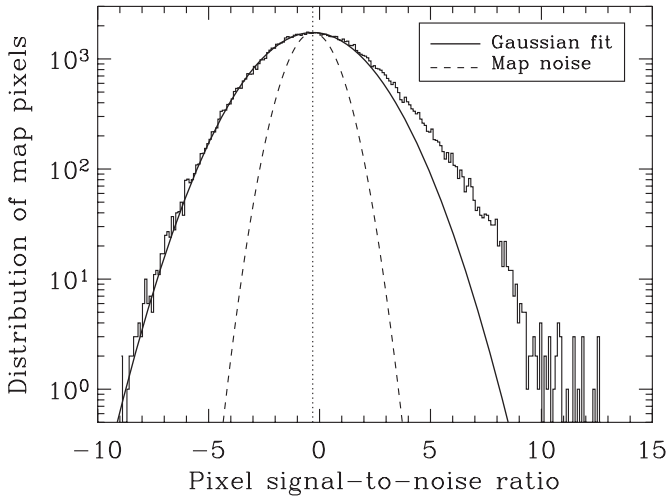

Figure 1. Distribution of the pixel S/N in BGS-Deep map at 500 μm (histogram). The scale on the *y*-axis is the number of pixels per bin of width 0.1. The positive tail is due to bright sources in the map. Because the map has a mean of zero, the peak of the distribution is shifted to the left of zero, as indicated by the vertical dotted line. A Gaussian (thick solid curve) is fit to the negative side of the histogram. For reference, the measured instrument noise (a Gaussian, with width 1.0 in units of S/N) is overplotted (thin dashed line). The map is clearly dominated by confusion noise.

both instrumental noise and confusion, $\sigma_{\rm conf}$. We estimate the confusion noise by subtracting the instrumental noise from the map rms in quadrature, $\sigma_{\rm conf} = \left(\sigma^2_{\rm map} - \sigma^2_{\rm inst}\right)^{1/2}$. The map rms is 16 mJy, and the median instrument noise is 6.6 mJy; thus, we conclude that the noise due to source confusion is $\sigma_{\rm conf} = 15$ mJy at 500 μm. Similar analyses give confusion noises of 17 and 21 mJy based on instrumental noises of 8.6 and 11 mJy at 350 and 250 μm, respectively. The maps are clearly dominated by confusion; this consists of a high-S/N measurement of the shape produced by galaxies, which are too close together to be resolved individually.

2.2. External Catalogs and Data

In order to estimate the contribution of sources in the BLAST maps to the CIB, we stack the map at positions from catalogs measured at other wavelengths. In the following subsections, we describe these external catalogs. The details of the stacking method are described in Section 3.1.

2.2.1. FIDEL/SIMPLE

Recently, it has been shown that deep Multiband Imaging Photometer for *Spitzer* (MIPS) 24 μm catalogs contain significant fractions of the sources that produce the CIB at 70 and 160 μm (Dole et al. 2006) and 850 μm (Wang et al. 2006), wavelengths that bracket the BLAST coverage. The deepest 24 μm catalog in BGS-Deep has been produced by Magnelli et al. (2009), combining GOODS-S with Far-Infrared Deep Extragalactic Legacy survey (FIDEL) data that cover a total of 0.21 deg^2. The FIDEL catalog was constructed using a higher resolution Infrared Array Camera (IRAC) catalog as a positional prior. This deep catalog from SIMPLE (*Spitzer* IRAC/MUSYC Public Legacy in ECDF-S; Gawiser et al. 2006) enabled the deblending of sources with separations as small as 0.5 FWHM in the MIPS map, resulting in an extremely faint flux density limit $S_{24} \gtrsim 15$ μJy. The faintest source in the catalog has $S_{24} = 13$ μJy, but the detections at $S_{24} < 30$ μJy should be considered tentative. The effects of this are discussed in Section 4.5.

Furthermore, since the catalog is a 24 μm-detected subset of SIMPLE, there also exist IRAC 3.6, 4.5, 5.8, and 8.0 μm flux densities for each object. The depth, reliability, and wavelength coverage of this catalog have been essential to this work.

2.2.2. MUSIC

Unlike the FIDEL catalog which has a fairly simple mid-IR selection function, the MUltiwavelength Southern Infrared Catalog (MUSIC) uses a near-IR selection with a much more heterogeneous data set combining ACS and IRAC maps with ground-based *JHK* Very Large Telescope (VLT) data and optical spectroscopy (Grazian et al. 2006). The primary use of this catalog is to obtain spectroscopic and optical photometric redshifts, although we also check the contribution to the CIB using stacking.

2.2.3. SCUBA

We extend the measurements made here with BLAST to lower frequencies using SCUBA data. The largest deep extragalactic SCUBA observations are in the GOODS North (GOODS-N) field. Data from this field have already been used to measure the 850 μm contribution to the CIB (Wang et al. 2006; Pope 2007), but, for consistency, we perform our own analysis using techniques identical to what we have done with the BLAST data. The map used here was produced by Borys et al. (2003), combining data from several different groups, and extended by Pope et al. (2005), covering an area of approximately 0.06 deg^2.[16] The noise in these maps is not uniform, varying from approximately 0.5–4 mJy. The existing *Spitzer* catalogs in GOODS-N (Papovich et al. 2004) are of similar depths to the FIDEL catalogs of GOODS-S. The size of the SCUBA and 24 μm overlap region in GOODS-N is 0.055 deg^2.

3. METHODOLOGY

3.1. Stacking

Determining the mean flux density of a population of sources that are individually too dim to be detected by examining their effect on a confusion-limited map is not new. The main approach goes by the name of "stacking." Because this work makes such heavy reliance on the technique, and because technical questions arise about the generalization to very high source density or the wisdom of excluding bright sources, etc., we review the basis of the technique here. We find that many of these misconceptions are avoided when one realizes that the technique is really one of taking the *covariance* of the map with the catalog.

Imagine we have a map of the sky, where D^j is the flux density in each pixel j after convolution with the instrumental point-spread function. Suppose also that we have one or several independent catalogs of sources made from other experiments; catalog C_α has N^j_α sources in pixel j, and we would like to know the mean flux density, S_α, of the sources in C_α. We denote the mean of N^j_α as μ_α, the average number of sources per pixel in list C_α. If all sources in a catalog produce identical flux density, S_α, then, along with whatever else is in the sky, there will on average be a contribution of $S^j_\alpha = S_\alpha N^j_\alpha$ to each pixel.

The BLAST maps have zero mean. We can write the flux density in the map as

$$D_j = S_1\left(N^j_1 - \mu_1\right) + S_2\left(N^j_2 - \mu_2\right) + \cdots + w_j, \qquad (1)$$

[16] The SCUBA map of GOODS-N used in this paper is available at http://www.noao.edu/staff/pope/DATA/SCUBA.html.

where w_j is the contribution of detector noise in pixel j, and, strictly speaking, S_α form the complete set of all objects in the universe. We have suppressed the mean by subtracting the $S_\alpha \mu_\alpha$ for each catalog from every pixel. We additionally require that w_j has a mean of zero. We imagine that the sources in the catalog are not correlated, such that N_α^j is a random, Poisson-distributed number. Furthermore, assume that no two lists are correlated, so that

$$\left\langle \left(N_\alpha^j - \mu_\alpha\right)\left(N_\beta^j - \mu_\beta\right)\right\rangle = 0, \qquad \forall\, \alpha \neq \beta. \tag{2}$$

Our goal is to determine the mean BLAST flux density per source in list C_α from knowledge of the BLAST maps, D_j, and the locations, N_α^j, of the sources in C_α, but without any other information, and in particular without requiring any knowledge of other lists C_β ($\alpha \neq \beta$).

N_j is a function that has a shape on the sky, and measuring the amplitude of this shape in the map determines S_α, the mean source brightness. The covariance of D_j with N_j provides the maximum-likelihood estimate[17] of this amplitude:

$$\begin{aligned}\mathrm{Cov}\left(D_j, N_\alpha^j\right) &= \frac{1}{N_{\mathrm{pix}}}\sum_j D_j N_\alpha^j \\ &= \frac{S_\alpha}{N_{\mathrm{pix}}}\left(\sum_j \left(N_\alpha^j\right)^2 - \mu_\alpha \sum_j N_\alpha^j\right) \\ &= S_\alpha \sigma^2_{N_\alpha^j},\end{aligned} \tag{3}$$

where N_{pix} is the total number of pixels in the map, and we have dropped terms in $N_\alpha^j N_\beta^j$ and $N_\alpha^j w_j$, which vanish in the sum. The first equality in Equation (3) holds because D_j has a mean of zero, and the last equality follows from the definition of variance. The variance of a Poisson distribution is

$$\sigma^2_{N_\alpha^j} = \mu_\alpha, \tag{4}$$

so the net result is that the zero-lag cross-correlation (covariance) of a catalog with the map divided by the mean number of sources per pixel is an estimate of the average flux density per source,

$$\hat{S}_\alpha = \frac{\mathrm{Cov}\left(D_j, N_\alpha^j\right)}{\mu_\alpha}. \tag{5}$$

A final rearrangement facilitates the use of Equation (5). Notice that the sum in Equation (3) runs over all pixels, with the weight of each pixel proportional to the number of catalog sources found within it, and that zero weight is given to pixels that do not contain a catalog source ($N_j = 0$). This can be rewritten as a sum, instead, over all catalog entries with unity weight,

$$\hat{S}_\alpha = \frac{1}{N_{\mathrm{pix}}\,\mu_\alpha}\sum_j D_j N_\alpha^j = \frac{1}{n_\alpha}\sum_k D_k, \tag{6}$$

where k is the index of sources in catalog C_α, D_k is the measured flux density in the map pixel that contains the kth catalog entry, and n_α is the total number of catalog entries, $n_\alpha = N_{\mathrm{pix}}\,\mu_\alpha$. This extraordinarily simple formula can be used to probe the properties of sources much too crowded to be detected individually, and also those with flux densities that are much fainter than the typical thresholds of source catalogs derived only from the map itself. Since the map pixel noises, w_j, are not uniform across the map, we weight the mean in Equation (6) by the inverse pixel variance to maximize the S/N of $\hat{S}_\alpha$. We explicitly subtract the weighted means of the BLAST maps.

Equation (6) provides a robust estimate of the mean brightness per source even when there are other, possibly substantial, contributors to the flux density present, C_β. This is provided that N_α^j is Poisson distributed, and N_α^j is not correlated with either the detector noise or sources in C_β. In other words, the effect of other sources on the estimator $\hat{S}_\alpha$ is to provide an additional source of noise. This noise may potentially be asymmetric, but it has a mean of zero, such that $\hat{S}_\alpha$ is unbiased.

Similarly, a catalog C_α can be subdivided into disjoint subsets, and the mean brightness due to each subset can be measured without bias. We use this fact to split up our catalogs based on IRAC colors and brightness at 24 μm.

We are now in a position to address the proper handling of sources that are bright enough to be easily recognized in the maps, for example, the sources in a BLAST 5σ catalog. We have shown that $\hat{S}_\alpha$, our estimate of S_α, is not affected by either the presence or the removal of flux density from other source lists C_β that are uncorrelated with C_α. However, since the sum of confusion noise and detector noise, $S_\alpha N_\alpha^j + w_j$, will cause sources near the threshold to be accidentally included or excluded from the BLAST catalog, any list made from the BLAST maps themselves will be artificially correlated with all the terms in Equation (1). Furthermore, since the BLAST-generated bright source catalog depends on the sum of the other terms in Equation (1), excision of the flux density from such a catalog will artificially correlate the remaining terms, such as $\left(N_\alpha^j - \mu_\alpha\right)$ and w_j. This introduces a bias in our estimator $\hat{S}_\alpha$ that is difficult to quantify. In all the following work, stacking is performed on the full BLAST maps, including any bright sources they contain.

We reiterate that that this formulation for stacking is slightly different than that used by other authors. In particular, Dole et al. (2006) performed aperture photometry on their stacked maps, effectively subtracting a local background. The stacking analysis performed by Pascale et al. (2009) uses a technique similar to that of Dole et al. (2006), and we have confirmed that their stacking calculations give results consistent with those presented here.[18]

The relation between the average BLAST flux density per source, S_ν, and the background specific intensity, I_ν, is $S_\nu n/\Omega$, where ν is the BLAST frequency and n/Ω is the number of sources per solid angle. Note that the intensity of the background is often defined through the product νI_ν, which is then related to νS_ν. In what follows, we use $I = \nu I_\nu$.

Near its faintest limit, any catalog is only partially complete, so we estimate n/Ω as $n_c/(C\Omega)$ where n_c is the number of catalog entries, C is the completeness of the catalog, assumed to be a function only of flux density, and Ω is the solid angle of the catalog. Completeness of the FIDEL 24 μm catalog is measured by comparing the differential flux density distribution

[17] This is the maximum-likelihood estimate only if the map pixel noises, w_j, are uniform. This is not the case for the BLAST maps. We address this issue later on.

[18] Pascale et al. (2009) use a slightly different reduction and spatial selection of the BLAST data than we use here, so we do not expect the results to be exactly the same.

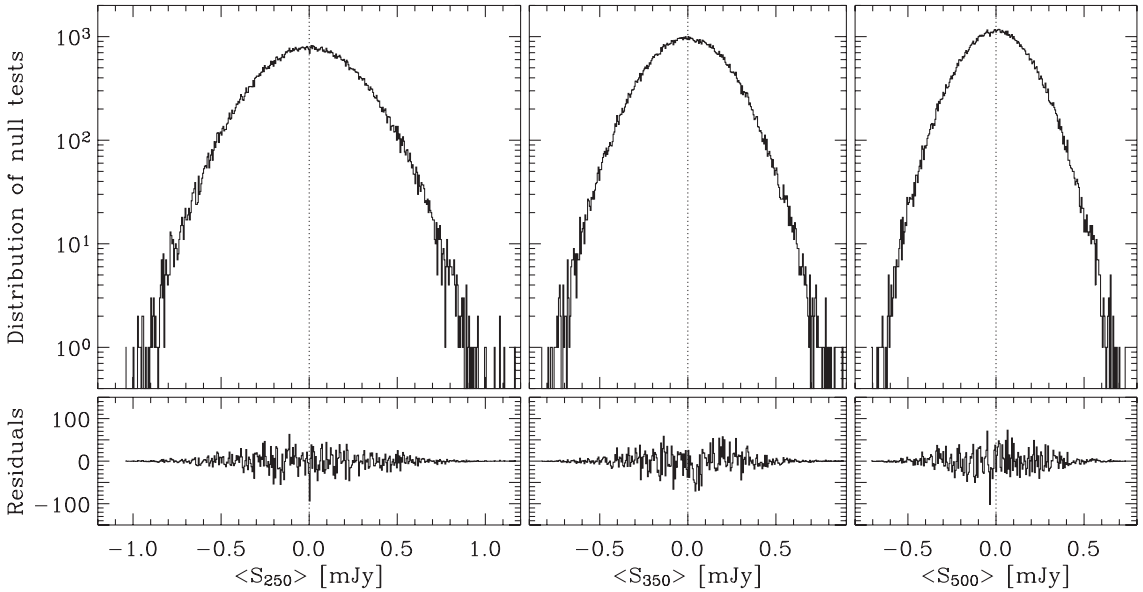

Figure 2. Quantification of errors in FIDEL stacking measurements. We calculate the average BLAST flux density at N random positions in the each map, where N is equal to the number of sources in the FIDEL catalog. Upper row: histograms of 10^5 stacking measurements at random positions. The scale on the y-axis is the number of simulations per 5 μJy bin. Lower row: difference between the histograms and the Gaussians centered at 0.0 with width equal to the rms of the distributions—clearly the histograms are very well described by Gaussians. We use the rms of these distributions as the errors in the stacked background values. We note that the errors between bands are strongly correlated, with Pearson correlation coefficients $\rho \sim 0.7$ (see Table 1) in all cases.

of the catalog to published completeness corrected counts. Above 400 μJy we use Shupe et al. (2008, Table 2) and between 35 μJy and 400 μJy we use Papovich et al. (2004, Table 2) after correcting their flux densities for a 5.6% difference in calibration that arises from choices in *Spitzer* photometry methods. The smooth function $C = [1 + (A/S_{24})^{\beta}]^{-1}$, where $A = 16$ μJy and $\beta = 1.8$, interpolates this correction. This correction is $C = 0.56$ at our lowest 24 μm flux density bin and has a small effect on our final result (see Section 4.2).

3.2. Uncertainties

To estimate the uncertainty of Equation (6) algebraically for a catalog C_α, one would need to know the scatter produced by its complement—the catalog of all sources not in C_α that contribute to the background (in addition to sources of instrumental noise). In practice, the complement is not known, so we establish the uncertainties and possible biases of our measurements by generating random catalogs and stacking them on the actual BLAST maps under analysis. We find, as expected, that the uncertainties are Gaussian distributed and scale as the map rms (including confusion noise) divided by the square root of the number of catalog entries. See Figure 2, and notice the high precision of achieving a null, i.e., zero inferred average flux density, from stacking on a catalog of random positions. The uncertainties arise from sampling the maps at random locations; since the confused flux density in the three separate BLAST maps is correlated, the uncertainties for stacking are correlated between BLAST bands. We measure the correlations from the simulations and find $\rho_{12} = 0.70$, $\rho_{13} = 0.68$, and $\rho_{23} = 0.70$, where ρ_{ab} is the Pearson correlation coefficient between bands a and b, and 1, 2, and 3 refer to 250, 350, and 500 μm, respectively.

3.3. Limitations of the Method

The stacked signals only return the mean source flux density if the catalog is Poisson distributed, since we have used the fact that the variance of the number of catalog entries in a region of a given size equals the mean. When this assumption is violated, the relation between the covariance of a map with a catalog and the corresponding mean flux density becomes complicated. If the catalog C_α is clustered at the scale of the BLAST beams, it is very easy to overestimate the mean flux density S_α, and therefore overestimate the contribution of a given catalog to the total sky intensity.

This problem is strikingly apparent when we perform the covariance with the MUSIC catalog, which has ~18,000 sources in 0.035 deg^2 (500,000 sources per square degree). We find that the background intensity inferred by stacking the BLAST maps on the MUSIC catalog exceeds the FIRAS values by factors of 2.5–3.0. We suggest that clustering in the catalog (whether due to selection biases or real clustering on the sky) is the cause of this overestimate.

The level of clustering that is measurable in a given area is strongly dependent on the source density, since, for a given level of clustering, the accuracy with which the mean can be measured goes as the square root of the number of sources in that area. We show here that the MUSIC catalog is strongly clustered at the scale of the BLAST beams and thus we should expect a biased measurement of the background, but that the FIDEL catalog, with ~9100 sources in 0.21 deg^2 (43,000 per square degree), is well behaved at the appropriate scales.

We have measured how close to Poisson distributed the MUSIC and FIDEL catalogs are. We place 500 circles of diameter D at random within the catalog area and count the number of catalog entries in each. Figure 3 shows the ratio of the variance to the mean as a function of circle diameter, for MUSIC and FIDEL. If the catalogs were uniform random distributions, this ratio would be unity. The MUSIC catalog shows a substantial excess variance at all angular scales above a few tens of arcseconds. It is not a surprise that galaxy locations are correlated and that MUSIC is deep enough to measure that. We also note that MUSIC is an extremely heterogeneous catalog, consisting of a variety of pointed observations. In contrast,

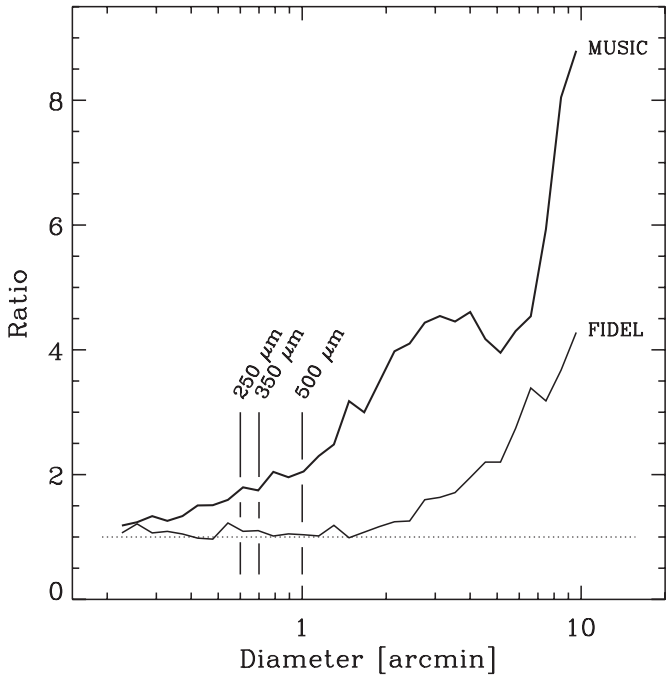

Figure 3. Clustering in the MUSIC and FIDEL catalogs as a function of scale. The ratio of the variance of the number of sources to the mean number of sources within a circle is plotted against the diameter of the circle for both the MUSIC and FIDEL catalogs. For a Poisson-distributed catalog, this ratio would be unity at all scales. Each point in the graph is the variance (divided by the mean) of the number of entries that fall within 500 randomly placed circles of a given size within the respective survey area. The broken vertical lines indicate the BLAST FHWMs. Notice that the FIDEL catalog retains a Poisson distribution to larger scales than the BLAST beams, while the much deeper and heterogeneous MUSIC catalog shows excess variance arising from the clustering of galaxies at all angular scales.

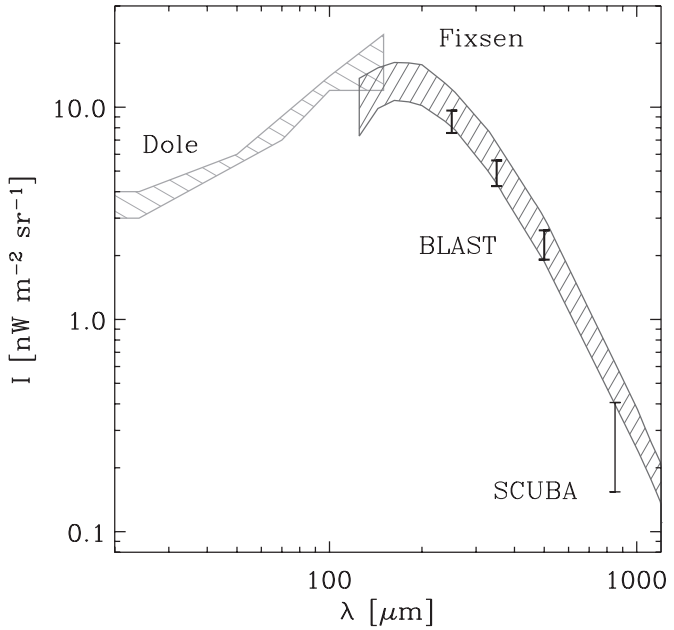

Figure 4. Total intensity of the far-IR background (CIB) in the BLAST bands associated with 24 μm galaxies is plotted against wavelength. The BLAST error bars include calibration uncertainties and are highly correlated between bands. The point at 850 μm labeled SCUBA is a similar stack in GOODS-N using data described in Borys et al. (2003) and Pope et al. (2005). The hatched region marked "Fixsen" is the absolute spectrum of the CIB determined from FIRAS observations on *COBE* (Fixsen et al. 1998). The hatched region at $\lambda \leqslant 160$ μm labeled "Dole" is the background reported by Dole et al. (2006) using a similar stacking analysis of *Spitzer* data in GOODS-N.

FIDEL is essentially a flux-limited catalog produced from a nearly uniformly sampled map. We conclude that on the angular scale of the BLAST beam sizes, one should anticipate that covariance with MUSIC will provide a biased estimator of total intensity.

The FIDEL catalog, which has a substantially lower surface density, does not show excess variance until scales of many arcminutes. We have tested whether this difference arises because FIDEL sources are intrinsically different from MUSIC sources, or is instead simply a feature of the shallower depth. We repeat the tests shown in Figure 3 for just the 1200 FIDEL sources that lie in the MUSIC region and for several random subsamples of 1200 MUSIC catalog entries. None of these curves is statistically distinguishable from unity at any angular scale, and we conclude that the Poisson variance associated with sampling MUSIC at the FIDEL number density dominates over the correlations in galaxy locations detected by MUSIC.

4. DISSECTING THE SUBMILLIMETER BACKGROUND

4.1. Total Intensity

We stack the BLAST maps on the FIDEL 24 μm catalog, using the methods described in Section 3.1. Completeness-corrected results are shown in Figure 4 and listed in Table 1, along with values of the CIB measured by Fixsen et al. (1998) and Dole et al. (2006). The BLAST measurements are consistent with having resolved 100% of the background, as measured by FIRAS. These numbers should be seen as lower limits, though; see Section 4.2. Even including calibration uncertainty, the BLAST total intensity values are twice as precise as FIRAS. In the rest of this paper, total intensity of the CIB refers to the BLAST values listed in Column 2 of Table 1. We note that while the completeness of the FIDEL catalog is uncertain (Section 3.1), the correction to the BLAST background intensities is small ($< 10\%$; see Section 4.2).

We examine the mean BLAST flux density per source as a function of 24 μm flux density by dividing the FIDEL catalog into bins of S_{24} (Figure 5). The brightest sources in the BLAST catalog are a factor of 10 times brighter than the mean brightness of 24 μm-selected sources shown in this figure; it is tempting to imagine that these curves extend to the right, but no brighter 24 μm sources exist. We conclude that the BLAST sources have anomalous $S_{\rm BLAST}/S_{24}$, yet the full $S_{\rm BLAST} \geqslant 3\sigma$ catalogs (Devlin et al. 2009) comprise only 10%–15% of the total intensity determined from stacking the full FIDEL catalog, since the number density of these objects is low.

The data do not allow a *linear* relation between flux density at 24 μm and flux density in the BLAST bands, such as any model of the form

$$S_{\rm BLAST} = A \left(\frac{\lambda_{\rm BLAST}}{24\,\mu{\rm m}} \right)^{p} S_{24}^{\beta}, \qquad (7)$$

with $\beta = 1$, would imply for any value of p. This suggests that the BLAST-detected light comes from a distribution of sources with different spectral energy distributions (SEDs), or with a range of redshifts that varies significantly as a function of S_{24}. This conclusion relies on the very large dynamic range, a factor of 500 in S_{24}, available from the FIDEL catalog. Even for a power-law relation, allowing β to differ from 1, the data do not support a constant value of β except perhaps at high flux densities. Figure 5 shows how the 250 μm curve diverges from $\beta = 0.5$ at low flux densities.

Table 1
Corrected Stacked Intensities

Band	BLAST			FIRAS
(μm)	Total (nW m^{-2} sr^{-1})	Low-z (nW m^{-2} sr^{-1})	High-z (nW m^{-2} sr^{-1})	(nW m^{-2} sr^{-1})
250	$8.60 \pm 0.59\,(1.04)$	$5.18 \pm 0.45\,(0.69)$	$3.42 \pm 0.37\,(0.50)$	10.4 ± 2.3
350	$4.93 \pm 0.34\,(0.68)$	$2.44 \pm 0.26\,(0.39)$	$2.49 \pm 0.21\,(0.37)$	5.4 ± 1.6
500	$2.27 \pm 0.20\,(0.36)$	$0.89 \pm 0.15\,(0.20)$	$1.38 \pm 0.13\,(0.22)$	2.4 ± 0.6

Notes. The quoted errors are measurement uncertainties only. The numbers in parentheses are errors including calibration uncertainties. The errors between the BLAST bands are strongly correlated because BLAST observes similar confusion-limited structure at all wavelengths. The Pearson correlation coefficients are $(\rho_{12}, \rho_{13}, \rho_{23}) = (0.70, 0.68, 0.70)$ for measurement-only uncertainties, where 1, 2, and 3 refer to 250, 350, and 500 μm, respectively. The coefficients for the full uncertainties are (0.90, 0.88, 0.91), (0.86, 0.80, 0.82), and (0.84, 0.83, 0.90) for the total, low-z, and high-z stacks, respectively. We note that these numbers are slightly different from those in Devlin et al. (2009), due to a small update in the calculation methods.

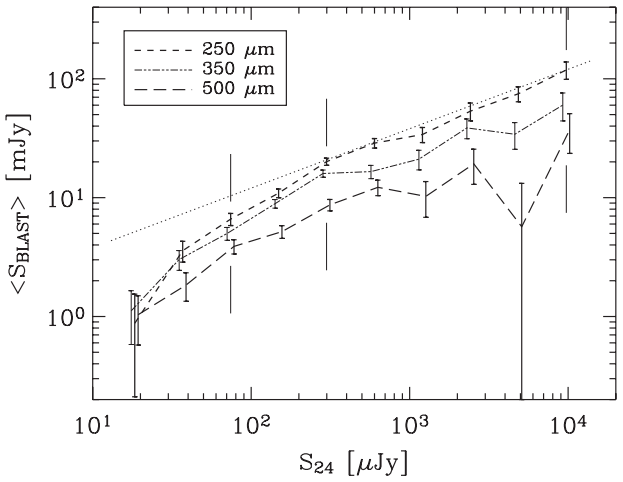

Figure 5. Mean BLAST flux density of FIDEL sources is plotted against 24 μm flux density for each of the three BLAST bands. The 350 and 500 μm curves have been horizontally displaced by -5% and $+5\%$, respectively, for visual clarity. The line near the uppermost curve is $S_{\rm BLAST} \propto S_{24}^{1/2}$, shown for reference. The vertical lines indicate the MIPS flux densities for which mean spectra are plotted in Figure 6. The number of FIDEL 24 μm sources per bin decreases from $\sim$2600 at the faint end to 3 at the bright end. The lowest flux density bins are based on tentative 24 μm detections, and are therefore biased low (see Section 4.5).

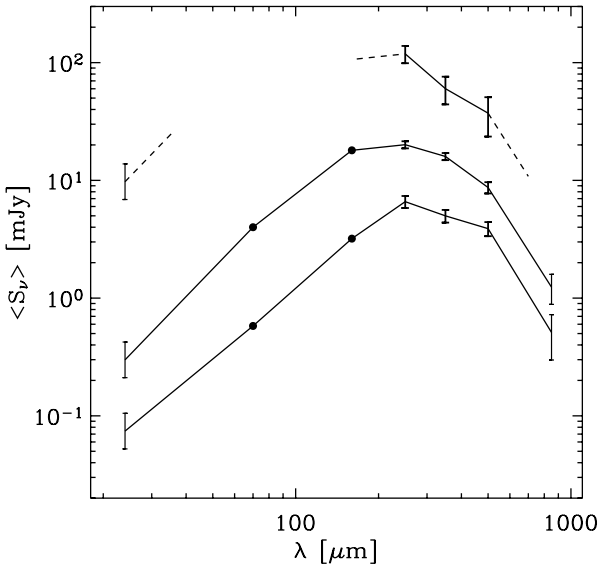

Figure 6. Spectra of the mean flux density in BLAST bands of sources of fixed 24 μm flux density. The three curves correspond to the 24 μm flux densities indicated by the three vertical lines in Figure 5. The point at 24 μm on each curve is the central flux density of the bin defining each subsample and the error bar indicates the width of that flux density bin. The circles at 70 and 160 μm on the lower two curves are the mean flux densities in those bins determined by a similar stacking analysis in Dole et al. (2006, Figure 7). For the upper curve, 70, 160, and 850 μm flux densities are not available, so we plot dashed lines following the same slopes as the middle curve. A clear trend of increasing mean flux density and apparent temperature (spectrum peaking at shorter wavelengths) is observed in the BLAST bands with increasing 24 μm flux density.

Spectra of the mean flux density in BLAST bands of sources at three fixed 24 μm flux densities are shown in Figure 6. This plot shows two features very clearly: first, that the average BLAST flux density is positively correlated with 24 μm flux density; and second, that fainter 24 μm sources appear cooler (as suggested by the shallower slopes through the BLAST wavelengths). This latter point is probably due to the fact that higher redshift sources have predominantly fainter 24 μm flux densities (see, for example, the strongly non-Euclidean region of the source counts at $S_{24} < 1$ mJy in Papovich et al. 2004)—if the average rest-frame galaxy dust temperature does not evolve appreciably, then the mean spectrum of fainter/more distant objects will undergo greater redshift and hence appear cooler. We note, however, that these curves are not well described by a single-object SED, and are certainly averages over a wide range of source types. The effects of a rough cut on redshift are presented in the next section, and detailed BLAST stacks as a function of redshift are explored in Pascale et al. (2009).

4.2. Division in Redshift

We use IRAC 3.6–8.0 μm flux densities of the FIDEL sources to make a cut in a color–color plane to broadly classify the sources as either high- or low redshift (Figure 7). The sources (small gray dots in the figure) mostly lie in two clouds, one in the lower-left quadrant and the other in the upper-left quadrant of the figure. For illustration, we overplot the observed colors of a galaxy template at a range of lookback times ($t_{\rm lb}$), ranging from 0 to 12 Gyr (black circles). The template is the SBc galaxy VCC 1987 from Devriendt et al. (1999), chosen because it is publicly available and exhibits the major features of the color–color space occupied by the FIDEL catalog. We note that the clouds correspond to regions of color–color space where this template galaxy lingers for several Gyr. The track traced out by the local star-forming galaxy M82, whose colors are thought to represent high-redshift submillimeter galaxies (Pope et al. 2008), is also shown. Its IRAC colors as a function of redshift are very similar to the SBc galaxy.

We adopt the line

$$([3.6] - [4.5]) = 0.0682 \times ([5.8] - [8.0]) - 0.075, \quad (8)$$

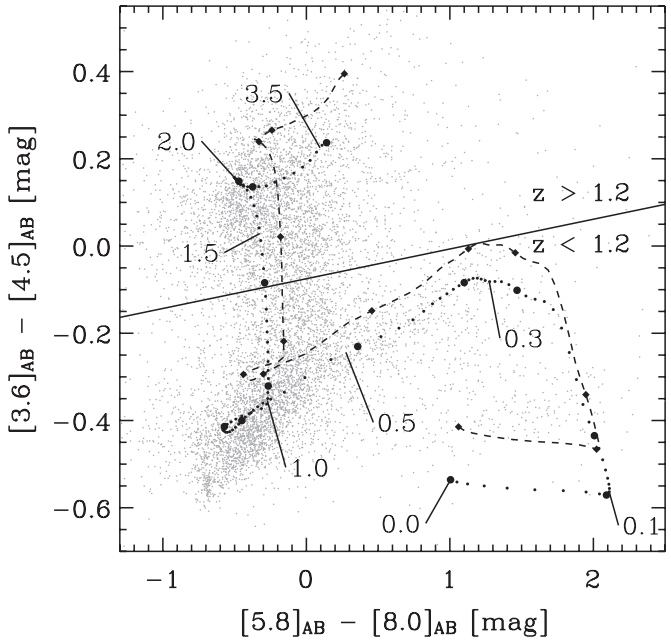

Figure 7. IRAC color–color plot for sources in the FIDEL catalog (small gray dots). The sources lie in two partially overlapping clouds. The black circles represent the colors of an SBc galaxy template (Devriendt et al. 1999, VCC 1987) observed at a range of redshifts. The circles are linearly spaced in lookback time; the small circles are spaced by 0.1 Gyr and the large circles by 1 Gyr. A range of redshifts are also indicated by the numbers along the track. The dashed line is the track traced out by the star-bursting galaxy M82. The diamonds indicate intervals of 1 Gyr, equivalent to the large circles for the SBc template. The solid line indicates the color cut used to separate high- and low-redshift sources—sources above the line are mostly at $z > 1.2$ while sources below the line are mostly at $z < 1.2$. The choice of this line is described in Devlin et al. (2009, supplement). We use $H_0 = 70.5$ km s^{-1} Mpc^{-1}, $\Omega_M = 0.274$, and $\Omega_\Lambda = 0.726$ (Hinshaw et al. 2009) to tabulate the lookback times.

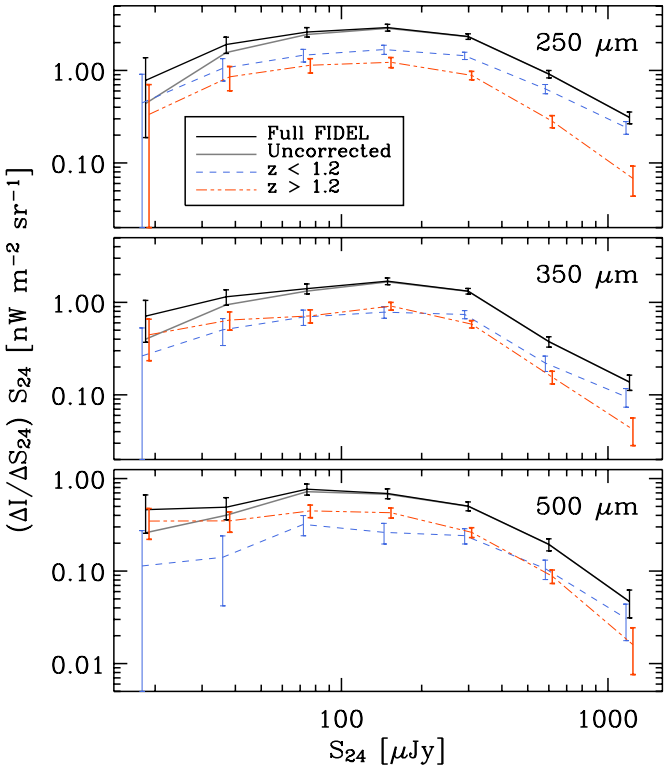

Figure 8. Completeness-corrected differential distribution of contribution to the CIB vs. flux density of the corresponding 24 μm galaxies. The result for the uncorrected differential stack is also shown for reference with a gray solid line to emphasize the fact that completeness only affects the two lowest bins. The 24 μm sources are divided into high- and low-redshift bins, as described in Section 4.2. The binning in 24 μm flux density is the same as in Figure 5, with the three highest flux density bins suppressed due to the small number of sources. The lowest 24 μm flux density bin is comprised of tentative detections, and so is possibly less certain than the error bars indicate (see Section 4.5). The low- and high-redshift curves have been horizontally displaced by −3% and +3%, respectively, for visual clarity.

(A color version of this figure is available in the online journal.)

where the quantities in square brackets are AB magnitudes in the IRAC bands, to divide the sources into two redshift bins. We have checked this cut for the 4242 sources in the MUSIC catalog for which spectroscopic or photometric redshifts are available, finding that sources lie at redshifts higher and lower than $z = 1.2$ above and below the line, respectively. The cut is remarkably sharp, with only 15% cross contamination (Devlin et al. 2009, supplement). This color–color cut is similar to the cut used by Yun et al. (2008, Figure 2) to identify submillimeter galaxy counterparts.

The differential contributions to the CIB from these "high" and "low" redshift sources as a function of 24 μm flux density are shown in Figure 8. We also show the corresponding curve for the total CIB (using the entire FIDEL catalog) for reference. Specifically, the stacks have been split into logarithmic bins in flux density and the total stacked intensity is determined for each bin, divided by the linear bin widths. We, therefore, plot $(\Delta I/\Delta S_{24})\, S_{24}$ as a function of S_{24}, where ΔI is the total contribution to the CIB at a given BLAST frequency from the sources in each bin and ΔS_{24} is the linear bin width.

The bulk of the CIB at 250 and 350 μm is clearly produced by sources with $S_{24} \geqslant 60$ μJy, while the low-flux density drop-off is less clear at 500 μm. This drop-off at low 24 μm flux density is due, in large part, to the number counts at 24 μm (Papovich et al. 2004, Figure 2), which are steepest at ∼200–1000 μJy and roll over significantly at lower flux densities. There appears to be CIB intensity missing from our measurements due to the flux density limit of the 24 μm catalog, in the sense that one would not expect strictly zero BLAST intensity in the next lower bin missing from each panel in Figure 8. We expect that this missing component is small. The 24 μm number counts below ∼20 μJy are uncertain, but since the 2σ upper limits derived from FIRAS are not much above the values derived in this analysis (Table 1), we conclude that there is no hidden population of very faint 24 μm sources that are important to the CIB at the BLAST wavelengths.

Two trends in redshift are clear: first, that the fraction of the total CIB due to high-redshift galaxies increases with wavelength through the BLAST bands (compare the relative heights of the dot-dashed and dashed curves in each panel); second, in all BLAST bands, the relative contribution to the background produced by high-redshift sources (i.e., observed to be colder) increases toward fainter 24 μm flux densities (compare the heights of the dot-dashed and dashed curves as a function of S_{24}). This analysis is consistent with our interpretation of Figure 6 described in Section 4.1.

Figure 9 shows the fraction of the CIB produced by the high-redshift sample as a function of wavelength. The curves are predictions from the phenomenological evolutionary model of Valiante et al. (2009). The different curves show the ratios of total intensities from galaxies brighter than $S_{24} = 30$ μJy (solid, dashed, and dot-dashed curves) and $S_{24} = 10$ μJy (dotted curve) from galaxies located at $z \geqslant z_c$, as labeled. We note that the curve for $z_c = 1.4$ is a substantially better fit than the curve for $z_c = 1.2$, despite the fact that photometric and spectroscopic

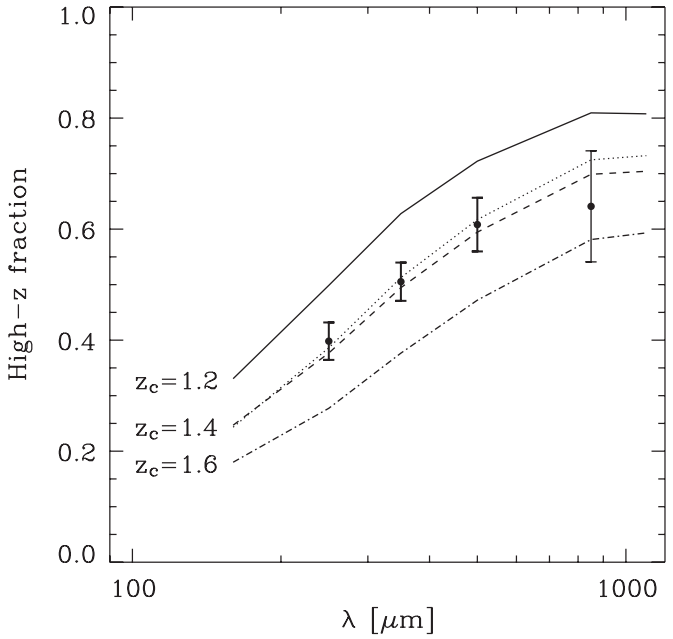

Figure 9. Fraction of the 24 μm-driven CIB which comes from high-redshift galaxies, as defined by the IRAC color–color cut shown in Figure 7, is plotted against wavelength for the three BLAST bands and SCUBA. Overplotted are predictions from the phenomenological evolutionary model of Valiante et al. (2009), for a range of redshift cuts. The solid, dashed, and dash-dotted curves are for a 24 μm catalog complete above $S_{24} = 30$ μJy. The dotted curve shows how the $z_c = 1.4$ curve changes for a $S_{24} \geqslant 10$ μJy catalog. $z_c = 1.2$ is clearly not a good fit to the data. We hypothesize that our estimate of z_c corresponding to the redshift cut of Section 4.2 is biased low due to selection effects. Note that the BLAST uncertainties are highly correlated (Table 1).

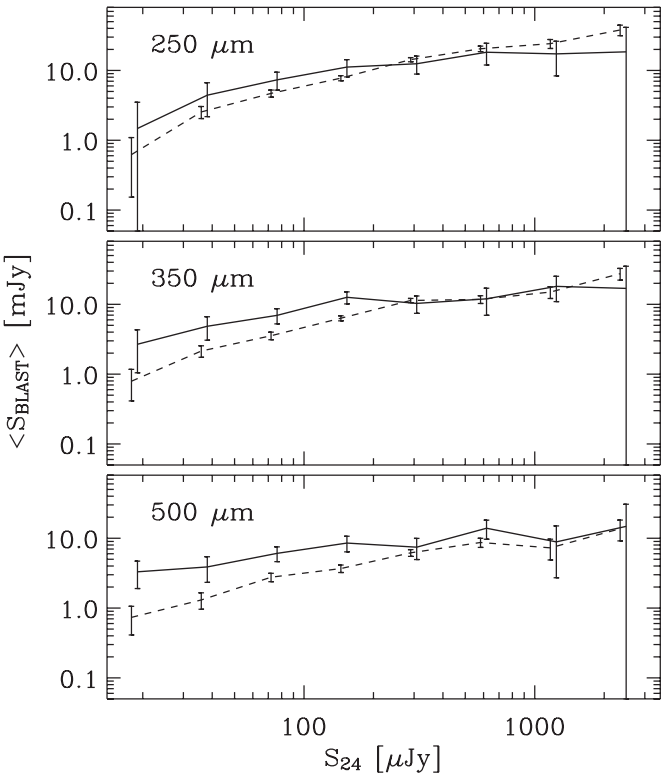

Figure 10. Average BLAST flux density of 24 μm sources classified as AGNs (solid lines) and for the full FIDEL list (dashed line). The classification is a color–color cut based on the power-law selection of Donley et al. (2008). The lowest flux density bins are based on tentative 24 μm detections, and are therefore biased low (see Section 4.5). The curves are horizontally shifted by +5% and −5% for clarity.

redshifts in the MUSIC catalog suggest that the IRAC color–color cut we have adopted corresponds to $z_c = 1.2$. Perhaps the subset of sources with redshifts from this training set is biased, and the galaxies dominating the stacks do, in fact, lie at slightly higher redshifts than the models suggest. We note that a similar IRAC color–color cut proposed by Yun et al. (2008) is designed to identify counterparts to 850 μm-selected galaxies that lie at redshifts predominantly $z > 2$. Alternatively, there are parameters governing the density and luminosity evolution of galaxies in the Valiante et al. (2009) model that could mimic this effect.

4.3. Galaxies Hosting an AGN

We attempt to select for active galactic nuclei (AGNs) in the FIDEL sample based on color–color cuts. We attempted to use the power-law selection suggested by Donley et al. (2008), but found that the majority of sources, even those that look like a power law through the IRAC bands, are rejected by the goodness-of-fit criterion, due to the small relative errors in the IRAC flux densities. The majority of sources that met both the power-law index and goodness-of-fit criteria were those with very poorly determined 5.8 and 8.0 μm flux densities, and thus landed all over the color–color plane. Instead, we make a cut on colors that encompasses all of the Donley et al. (2008) sources with minimal contamination from non-AGN:

$$y \geqslant 1.21\,x - 0.30, \tag{9}$$

$$y \leqslant 1.21\,x + 0.22, \tag{10}$$

$$y \geqslant -0.83\,x + 0.16, \tag{11}$$

where $y \equiv \log(S_{8.0}/S_{4.5})$ and $x \equiv \log(S_{5.8}/S_{3.6})$. We find that 480 FIDEL sources meet this criteria, which is similar to the expected number of X-ray-detected AGN, based on the source density reported by Luo et al. (2008). The average BLAST flux density at the positions of the IRAC color-selected sources is 7.5 ± 1.1, 7.4 ± 0.9, and 6.0 ± 0.8 mJy at 250, 350, and 500 μm, respectively. These values are significantly larger than for the full FIDEL list, 4.6 ± 0.2, 3.6 ± 0.2, and 2.3 ± 0.2 mJy.

Figure 10 shows the average BLAST flux density binned by 24 μm flux density for the FIDEL sources labeled as AGN (solid line) and for the full set (dashed line). We see that across all BLAST bands, the AGNs are brighter than average at all but the greatest 24 μm flux densities, with the ratio (averaged over all 24 μm flux densities) increasing from 1.6 to 2.6, from 250 to 500 μm. The fact that this fraction increases at longer wavelengths (under the assumption that higher redshift sources should appear cooler) is puzzling since the space densities of both AGNs and the ultra-luminous star-forming galaxies selected at 850 μm grow quickly to redshifts $z \sim 2$–2.5 (e.g., Chapman et al. 2005; Wall et al. 2005, 2008). Either the dust in star-forming galaxies is generally warmer than in the hosts of AGNs, or the total background produced by purely star-forming galaxies occurs at lower redshifts. This latter explanation is more likely, since it is now believed that the bulk of the total stellar mass in the universe was formed in more numerous, less luminous galaxies at lower redshifts than those detected in longer wavelength submillimeter surveys (e.g., Pérez-González et al. 2008).

For comparison, we also stack on catalogs of AGNs selected by the *Chandra X-ray Observatory* and by optical variability.

The X-ray sample of Luo et al. (2008) contains 462 sources, 164 of which (ignoring upper limits) fall in the region of the *R* band versus soft X-ray flux plot that is thought to select for AGN (Luo et al. 2008, Figure 12). The average BLAST flux density at the positions of the X-ray-selected AGN is 7.3 ± 1.9, 7.5 ± 1.5, and 5.3 ± 1.3 mJy at 250, 350, and 500 μm, respectively, similar to the values listed above. We note that the stack on the full list of 462 is marginally larger at 250 μm (9.4 ± 1.2 mJy), although nearly identical at 350 and 500 μm (7.6 ± 1.9 and 5.1 ± 0.8 mJy). The optical variability sample of Trevese et al. (2008) contains 132 objects, with average flux densities of 9.1 ± 2.1, 7.1 ± 1.7, and 4.4 ± 1.4 mJy at 250, 350, and 500 μm, respectively.

Our measurements are tantalizing since it is one of the major goals in modern cosmology to establish an evolutionary connection between the formation of the most massive galaxies and the growth of black holes. However, we warn the reader that the color–color selection described above may be significantly contaminated by star-forming galaxies, which would introduce strong biases such that the observed trends here may be unrelated to the underlying evolution in the AGNs and star-forming galaxy populations. A catalog of AGN which is complete and free of interlopers would allow us to improve our understanding of the relative importance of AGN in the formation of the CIB.

4.4. *BzK* Galaxies

Daddi et al. (2004) have shown that selecting galaxies that are dimmer in z band than they are in B and K_s yields a list which contains many star-forming galaxies. Specifically, *BzK* galaxies are those for which

$$\Delta_{BzK} \equiv (z - K)_{AB} - (B - z)_{AB} > -0.2, \qquad (12)$$

which tends to select star-forming galaxies at $z \geqslant 1.4$. Their association with ULIRGs has been studied (Daddi et al. 2005), and Hartley et al. (2008) conclude from their mild clustering properties that they are associated with dark matter halos.

We use photometry from the 1548 FIDEL sources with MUSIC catalog identifications to calculate Δ_{BzK}. There are 388 *BzK* galaxies in the region, while the BLAST 5σ catalog contains only a handful of entries, so we know that the *BzK* criterion is not selecting BLAST sources in general. Separating all 1548 FIDEL galaxies into bins by Δ_{BzK} and stacking on the galaxies in each bin we find only a very weak dependence of mean BLAST flux density on Δ_{BzK}. *BzK* galaxies, i.e., sources with $\Delta_{BzK} > -0.2$, are mildly brighter than others; the FIDEL/MUSIC *BzK* sources have average BLAST flux densities 1.3–1.7 times greater than for the full list, and produce $32\% \pm 6\%$, $34\% \pm 7\%$, and $42\% \pm 11\%$ of the total BLAST intensity at 250, 350, and 500 μm, respectively. It is clear that *BzK* samples make an important contribution to the CIB, but this is largely because they are so numerous.

For comparison, Takagi et al. (2007) find that *BzK* galaxies produce 9% of the CIB at 850 μm, as measured by FIRAS. If we restrict our sample to the galaxies with $K_S \leqslant 22.9$, the limiting magnitude of the Takagi et al. sample, we find that the *BzK* galaxies make up 12%, 10%, and 12% of the CIB at 250, 350, and 500 μm, respectively, comparable to Takagi et al.

4.5. Spurious Detections in FIDEL Catalog

As described in Section 2.2.1, detections in the FIDEL catalog below 30 μJy are considered tentative. This affects the lowest flux density bin in Figures 5, 8, and 10. Since Figures 5 and 10 are average flux densities, the effect of spurious sources (which are presumably uncorrelated with the BLAST maps) is to lower the estimate, so the lowest flux density bin is probably biased low. The uncorrected curves in Figure 8 are *sums* over the FIDEL sources, so spurious sources do not affect the measurement, and there is no bias. Spurious sources would affect the completeness correction, however, and thus the curves labeled "full FIDEL" should also be regarded as biased low. In addition, since the quoted uncertainties take into account the number of sources included in the stack, the error bars are likely smaller than they should be.

5. CONCLUSIONS

For the first time, we trace the full submillimeter intensity of the far-IR background using a specific catalog of 24 μm-selected galaxies. We use the properties of these 24 μm galaxies to analyze the composition of the CIB. We have determined that the average submillimeter flux density varies nonlinearly with 24 μm flux density; these results require that the underlying averaged SED evolves with redshift. We make precise measurements of how the fraction of the CIB produced at higher redshifts varies with the observed wavelength through the submillimeter spectrum. These values are lower than models predict. We determine the total submillimeter intensity from unresolved AGN using an IRAC color–color selection, finding weak evidence that they produce a non-negligible fraction of the CIB, and a relatively larger fraction in the longer wavelength BLAST bands. This result could be demonstrating that the epoch of peak star formation is at lower redshifts than the peak in AGN space density, which might be expected if most stars form in lower luminosity, lower redshift galaxies than the ultra-luminous star-forming galaxies selected at 850 μm. However, this result strongly depends on the AGN selection criterion which may contain many sources without an AGN, and which is also expected to be incomplete at higher redshifts. We also stacked at the positions of *BzK* galaxies, finding that they contribute 32%–42% of the CIB in the BLAST bands, consistent with the contribution found by Takagi et al. (2007) at 850 μm when the depths of the optical catalogs are considered.

Thanks to Alex Pope for providing the SCUBA GOODS-N map, and to J. E. G. Devriendt for providing model galaxy spectra. We acknowledge the support of NASA through grant numbers NAG5-12785, NAG5-13301, and NNGO-6GI11G, the NSF Office of Polar Programs, the Canadian Space Agency, the Natural Sciences and Engineering Research Council (NSERC) of Canada, and the UK Science and Technology Facilities Council (STFC). This research has been enabled by the use of WestGrid computing resources. This work is based in part on observations made with the *Spitzer Space Telescope*, which is operated by the Jet Propulsion Laboratory, California Institute of Technology under a contract with NASA.

REFERENCES

Barger, A. J., Cowie, L. L., Sanders, D. B., Fulton, E., Taniguchi, Y., Sato, Y., Kawara, K., & Okuda, H. 1998, Nature, 394, 248
Blain, A. W., Ivison, R. J., & Smail, I. 1998, MNRAS, 296, L29
Borys, C., Chapman, S., Halpern, M., & Scott, D. 2003, MNRAS, 344, 385
Chapman, S. C., Blain, A. W., Smail, I., & Ivison, R. J. 2005, ApJ, 622, 772
Coppin, K., et al. 2006, MNRAS, 372, 1621
Cowie, L. L., Barger, A. J., & Kneib, J.-P. 2002, AJ, 123, 2197
Daddi, E., Cimatti, A., Renzini, A., Fontana, A., Mignoli, M., Pozzetti, L., Tozzi, P., & Zamorani, G. 2004, ApJ, 617, 746

Daddi, E., et al. 2005, ApJ, 631, L13
Devlin, M. J., et al. 2009, Nature, 458, 737
Devriendt, J. E. G., Guiderdoni, B., & Sadat, R. 1999, A&A, 350, 381
Dole, H., et al. 2006, A&A, 451, 417
Donley, J. L., Rieke, G. H., Pérez-González, P. G., & Barro, G. 2008, ApJ, 687, 111
Fixsen, D. J., Dwek, E., Mather, J. C., Bennett, C. L., & Shafer, R. A. 1998, ApJ, 508, 123
Gawiser, E., et al. 2006, ApJS, 162, 1
Grazian, A., et al. 2006, A&A, 449, 951
Griffin, M., et al. 2007, Adv. Space Res., 40, 612
Hartley, W. G., et al. 2008, MNRAS, 391, 1301
Hauser, M. G., & Dwek, E. 2001, ARA&A, 39, 249
Hinshaw, G., et al. 2009, ApJS, 180, 225
Holland, W. S., et al. 1999, MNRAS, 303, 659
Hughes, D. H., et al. 1998, Nature, 394, 241
Knox, L., Cooray, A., Eisenstein, D., & Haiman, Z. 2001, ApJ, 550, 7
Knudsen, K. K., van der Werf, P. P., & Kneib, J.-P. 2008, MNRAS, 384, 1611
Luo, B., et al. 2008, ApJS, 179, 19
Magnelli, B., Elbaz, D., Chary, R. R., Dickinson, M., Le Borgne, D., Frayer, D. T., & Willmer, C. N. A. 2009, A&A, 496, 57
Papovich, C., et al. 2004, ApJS, 154, 70
Pascale, E., et al. 2008, ApJ, 681, 400
Pascale, E., et al. 2009, ApJ, 707, 1740
Patanchon, G., et al. 2008, ApJ, 681, 708
Patanchon, G., et al. 2009, ApJ, 707, 1750
Pérez-González, P. G., et al. 2008, ApJ, 675, 234
Pope, E. A. 2007, PhD thesis, The Univ. of British Columbia, Canada
Pope, A., Borys, C., Scott, D., Conselice, C., Dickinson, M., & Mobasher, B. 2005, MNRAS, 358, 149
Pope, A., et al. 2008, ApJ, 675, 1171
Puget, J.-L., Abergel, A., Bernard, J.-P., Boulanger, F., Burton, W. B., Desert, F.-X., & Hartmann, D. 1996, A&A, 308, L5
Scott, S. E., et al. 2002, MNRAS, 331, 817
Serjeant, S., et al. 2008, MNRAS, 386, 1907
Shupe, D. L., et al. 2008, AJ, 135, 1050
Smail, I., Ivison, R. J., Blain, A. W., & Kneib, J.-P. 2002, MNRAS, 331, 495
Takagi, T., et al. 2007, MNRAS, 381, 1154
Trevese, D., Boutsia, K., Vagnetti, F., Cappellaro, E., & Puccetti, S. 2008, VizieR Online Data Catalog, 348, 80073
Truch, M. D. P., et al. 2009, ApJ, 707, 1723
Valiante, E., Lutz, D., Sturm, E., Genzel, R., & Chapin, E. 2009, ApJ, 701, 1814
Viero, M., et al. 2009, ApJ, 707, 1766
Wall, J. V., Jackson, C. A., Shaver, P. A., Hook, I. M., & Kellermann, K. I. 2005, A&A, 434, 133
Wall, J. V., Pope, A., & Scott, D. 2008, MNRAS, 383, 435
Wang, W.-H., Cowie, L. L., & Barger, A. J. 2006, ApJ, 647, 74
Yun, M. S., et al. 2008, MNRAS, 389, 333